Ionospheric Interaction Based Detection of Sub-centimeter Space Debris

Ian M. DesJardin, Christine M. Hartzell
University of Maryland, College Park
Department of Aerospace Engineering

ABSTRACT

Detection of space debris below the size limits of optical and radar-based methods (<1cm) is an open question. All previous detection attempts in this size range have relied on in situ measurements. This limits the results to qualitative surveys, not operational catalogs. A new method of detecting orbital debris is being developed that detects debris-space plasma interactions as a proxy for detecting the debris directly. Natural stable plasma wave emissions, known as solitons, and a wake are generated by these interactions [1,2]. Proposed detection approaches of plasma solitons include incoherent scatter radar (e.g. EISCAT 3D [3] & HAARP) and spacecraft measurements (e.g. Swarm-E RRI instrument [4]). We propose a new detection method for these local plasma structures based on measurements of GNSS carrier frequency or another known space-to-Earth radio transmission. This approach uses passive ground-based receivers which makes it amenable to continuous surveying.

Our analysis uses the Appleton-Hartree equation to predict radio signal distortion indicative of local plasma structures. For frequencies above the ionospheric plasma frequency, this manifests as a refractive phase advance and scattering of the signal. For sub-centimeter debris, we show that the forward scattering cross section from the plasma wake is larger than the Rayleigh cross section. Both can be larger than the backscatter from a ground radar. This scattering analysis is then used to estimate the ground receiver spacing necessary to resolve the scattering from a wake and/or an ion acoustic soliton. Ion acoustic solitons from the upper ionosphere are the most likely to be observed. Bright astronomical radio sources are also surveyed to use in lieu of GNSS signals. Existing ground stations are surveyed. We also estimate the magnitude of refractive phase advance by a characteristic plasma wake of the International Space Station superimposed on the International Reference Ionosphere (IRI) model and identify GPS receivers capable of detecting this effect. This experiment could test the physics of the technique.

1. INTRODUCTION

Space debris is an exponentially growing risk for operating in Earth orbit. Mega-constellation projects may compound the existing debris population. Thus, the need to track and understand the debris population below the currently trackable threshold (<1cm) is important to space sustainability. This paper suggests a new detection strategy for detecting this population based on ionosphere-spacecraft interaction. From 50-2000 km altitude there is a layer of ionized atmosphere that arises from solar UV radiation ionizing the neutral atmosphere known as the ionosphere. The amount of plasma, characterized by the electron density n_e, strongly depends over several orders of magnitude on the day/night cycle, latitude, and solar cycle which all change the local flux of UV radiation. In general, the ionosphere consists of several layers that are larger during the day than at night. The area with the largest n_e is the F-layer which often has a midpoint altitude of around 300-500 km [4,5]. In this work, we shall use a characteristic model of ionosphere which accounts for cyclic variations. Specifically, we use the International Reference Ionosphere-2020 (IRI), managed by the Committee on Space Research (COSPAR) and the International Union of Radio Science (URSI).

Spacecraft interact with the ionosphere to create plasma waves and density structures around the spacecraft. When a conductive material is immersed in a plasma, the higher mobility of electrons will cause the material to become negatively biased relative to the surrounding plasma. Dysfunctional debris does not exercise active spacecraft potential control. The biased spacecraft will electrically disturb the local plasma flow. The boundary layer which forms from the surface to the free stream of the plasma is called the plasma sheath of comparable length scale to the Debye length, λ_D, defined for a quasineutral cold plasma in SI units as $\lambda_D = \sqrt{\frac{\epsilon_0 k T_e}{n_e e^2}}$ where ϵ_0 is the permittivity of free space, k_B is the Boltzmann constant, and e is the charge of an electron. This excites plasma waves and shock-

like structures which can either stay attached to the spacecraft or detach from it. Numerous physical models have been proposed for predicting what waves get created in what flow conditions [1,2,6–8]. There have been in situ observations of these structures [9,10]. We consider two such structures: the plasma wake and ion acoustic solitons. In the ionospheric plasma, orbital speeds are often supersonic relative to the ion acoustic speed but subsonic relative to the electron acoustic speed. Behind the direction of motion of the spacecraft a wake will form where the plasma density is lower than the undisturbed plasma. Ion acoustic solitons are nonlinear waves with density perturbations which can form under a range of ion acoustic Mach numbers. They are stable under collisions with other solitons and can propagate for great distances. Radio propagation through a plasma is strongly influenced by the local properties of the plasma. The index of refraction in a plasma neglecting magnetic and Landau damping effects is given by Eqn. 2.1. This is known as the Appleton-Hartree equation. ω_0 is the plasma frequency where $\omega_0 = \sqrt{\frac{n_e e^2}{m_e \varepsilon_0}}$ in SI units. Definitionally, the index of refraction squared is the relative permittivity.

$$\varepsilon_r = n^2 = 1 - \frac{\omega_0^2}{\omega^2} \tag{2.1}$$

n is a function of the local electron density ($n_e(\boldsymbol{x})$). Local structure in $n(\boldsymbol{x})$ will lead to classical optics phenomena such as scattering and refraction resulting from the changing electron density. Thus, radio wave propagation will be affected when transmitted through the electron density variations that are generated by the passage of a spacecraft or piece of debris. This predicted modification of radio waves may provide an alternate method to detect debris, rather than traditional methods that rely on directly observing the debris itself. In this study, we focus on GNSS signals as the probing radio transmission because they have global coverage and are well characterized. However, this technique is not unique to GNSS signals. Ionospheric disturbances have been indirectly observed by radio telescopes using astronomical radio sources. Astronomical radio sources include Sagittarius A [11,12], supernova remnants (such as Cassiopeia A [13] and the Crab Nebula [14]), and radio galaxies [15]. In particular, Cassiopeia A has been studied at 25.19 MHz [16]. The largest modifications to the Appleton-Hartree equation occur when $\omega \approx \omega_0$. Fig. 1 shows a characteristic night and day cycle of the ionosphere. The color indicates the local plasma frequency calculated from the ionosphere generated electron density. The plasma frequency varies from 1-10MHz. Thus, astronomical sources closer to 10MHz may be more suitable for detecting ionospheric disturbances than L-band GNSS signals (near 1 GHz). Table 1 summarizes the carrier frequencies of common GNSS systems. In our scattering models, we will use 25.19 MHz as a candidate frequency since this extremizes operating near the plasma frequency.

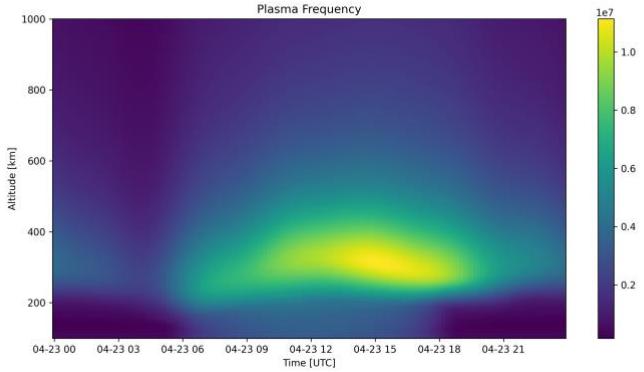

Fig. 1: Plasma frequency predicted by the 2012 IRI on April 23, 2019 at 0°latitude and 0° longitude.

Table 1: Carrier frequencies of common GNSS systems.

Carrier	Frequency (MHz)
GPS L1	1575.42
GPS L2	1227.60
GPS L3	1381.05
GLOSNASS L1	1602.0
GLOSNASS L2	1246.0
BeiDou B1	1575.42

BeiDou B2	1191.795
BeiDou B3	1268.52
Galileo E1	1575.42
Galileo E5	1191.795
Galileo E6	1278.75

Scattering theory has been derived from the Appleton-Hartree equation [17]. The theory was created in response to observations of Sputnik 1, Explorer 1 & Explorer III scattering over-the-horizon radio broadcasts at night which were highly dependent on background ionosphere conditions. These bursts were used to track early satellites [18–21] to varying degrees of success. How often these bursts would happen and whether they could always be attributed to spacecraft flying overhead was debated at the time [22].

It has also been shown that GNSS, specifically GPS, can be used as a bistatic radar on satellites. The very weak signal-to-noise ratio which comes from the scattered GNSS signal from small targets is a challenge. However, this can be overcome through novel signal processing techniques which utilize the doppler shift of targets orbiting faster than a GNSS source to disentangle the scattered signal [23]. We use the relative signal strength of the scattered GNSS signal from this line of work to set a relative signal strength which could be detected.

2. REFRACTIVE EFFECTS

The Appleton-Hartree equation (Eqn. 2.1) establishes that there is a highly frequency dependent index of refraction in a plasma. The tropospheric and multipath components to GNSS system errors do not exhibit a frequency dependent behavior. In multi-frequency systems, such as GPS, the phase difference between the carrier signals allows for estimation of the plasma-only phase delay. The total ionospheric plasma contribution to the phase delay is commonly expressed as the total electron content, $TEC \overset{\text{def}}{=} \int n_e ds$ which can be related to the actual phase by $\delta\rho = -\kappa\frac{TEC}{f^2}$. κ is a grouping of physical constants set in [24] to $\kappa = 40.309$ in SI units. TEC is derived from the Appleton-Hartree equation [24]. TEC is defined as a path integral along the radio propagation. Local modifications to the electron density from spacecraft-ionospheric interactions will change the phase delay. Commercially available ionospheric research GNSS receivers, such as the Septentrio PolaRx5S Scintillation Reference Receiver, advertise carrier phase accuracy of 1mm on GPS L1 and L2 at 1 Hz.

The contribution to total electron content from a Gaussian electron density perturbation $\left(\delta n_e = n_{e,background} U_{max} \exp\left(-\left(\frac{x}{w}\right)^2\right)\right)$ is given by $\delta TEC = \int \delta n_e ds = n_{e,background} U_{max} w \sqrt{\pi}$ where w is the width of the pulse and U_{max} is the relative depletion of the background. We take $U_{max} = 0.99$ which is consistent with observations of the Space Shuttle wake [25]. It should be noted that the Space Shuttle wake was observed to be Mach cone shaped [25], however we still assume the wake is Gaussian shaped to make the math more tractable. This is justified by noting that the transverse line integral through a Mach cone will resemble a 1D Gaussian with a width depending on the relative angle of the Mach cone and the incident radio beam.

We wish to compare the phase advance from the local plasma structure to the precision of carrier phase measurement in ground receivers to establish if this effect would be detectable. For our radio receiver, the intrinsic thermal noise can be expressed as $N = BW\ k_B T_{sys}$ where BW is the bandwidth, k_B is the Boltzmann constant, and T_{sys} is the effective noise temperature of the system. Typical GPS systems have a receiver noise of $263\ K$ [26]. A related signal strength quantity is the carrier-to-noise ratio (c/n_0) expressed in dB-Hz. $n_0 \overset{\text{def}}{=} \frac{N}{BW} = k_B T_{sys}$. c is the carrier signal. For a phased lock loop (PLL), commonly used in GNSS system carrier wave tracking, the expected accuracy of the carrier phase is given by Eqn. 2.1 where τ is the prediction integration time and λ is the wavelength. The right-hand side of the equation is a good approximation for strong signal strength.

$$\sigma_{PLL} = \sqrt{\frac{BW}{c/n_0}\left[1 + \frac{1}{2\tau \cdot c/n_0}\right]}\frac{\lambda}{2\pi} \approx \sqrt{\frac{BW}{c/n_0}}\frac{\lambda}{2\pi} \tag{2.1}$$

Good GNSS reception is $c/n_0 = 45$ dB $-$ Hz. Since $\tau \gg 1/(2\ c/n_0)$, $\tau \gg 20\ \mu s$ preventing a PLL from resolving events faster than the integration time. GNSS spacecraft/debris-based transient effects would last longer than that. At a loss of -200 dB, $c/n_0 = -155$ dB $-$ Hz making $\sigma_{PLL} \approx 10^9\ m$. The phase would be untraceable for the weakly scattered signal. The integration time necessary would also be enormous. However, the scattering region is small enough that the debris must be in the line of sight between the ground station and the GNSS transmitter.

We will also examine the use of radio telescopes as the ground receiver in lieu of GNSS receivers. Radio telescopes publish their "system equivalent flux density" (SEFD) in units of Jansky where 1 Jansky = $10^{-26}\frac{W}{m^2-Hz}$. Similarly, the intensity (I) of astronomical sources is published in units of Jansky. For radio telescopes, the phase measurement performance becomes:

$$\sigma_\phi = \sqrt{\frac{SEFD}{I}}\frac{\lambda}{2\pi} \tag{2.2}$$

When a plasma wake / GNSS transmitter occultation occurs, it is expected that there will be a transient phase effect in the carrier frequency. In extreme cases, this would result in GNSS phase scintillation which has been observed for large scale ionospheric irregularities [5]. We will show that, for small debris, this effect is expected to be observable from radio telescopes but not necessarily ionospheric monitoring GNSS stations. In Section 5, we show that for larger objects an existing commercial ionospheric monitoring GNSS stations could be used as a sensor. We outline an experiment to test this.

At solar maximum on GPS L2 frequency, we suppose a $5cm$ sized debris object forms a Gaussian wake with width of $50\ cm$ and maximum magnitude equal to the background at the F_2 layer peak ($n_e = 1.7\ \times 10^{12}\ m^{-3}$). The width of the Gaussian representing the wake relative to the radius of the object (10x) is of the order of a spherical object's Mach 8 wake length [17]. To be precise one would need to be specific about geometry, local ion acoustic Mach number, and angle of radio line of sight relative to the wake axis. The wake would change the TEC by $\delta TEC = \int n_e ds = 1.5\ \times 10^{12}\ m^{-2}$ and the phase by $|\delta\phi| = \kappa\frac{\delta TEC}{f^2} = 40\ \mu m$. This is still orders of magnitude smaller than the $1mm$ precision of existing GNSS reference receivers. At the Allen Telescope Array (ATA) run by SETI, GPS L1 frequency was measured to have a flux density of $10^{-18.1}\frac{W}{m^2-Hz} = 7.9\ \times 10^4\ kJy$ [27]. The SEFD in the L-band was published to be $\sim 10\ kJy$ [28]. ATA should be able to observe GPS carrier frequencies to $\sigma_\phi \approx 0.4\ mm$. The L-band SEFD for the Very Large Array (VLA) (link) and Greenbank telescopes (link) are even smaller. Therefore, at L-band frequencies, we expect that some radio telescopes observing GNSS carrier frequencies should be sensitive to wakes from multiple centimeter sized debris.

We can carry out a similar exercise for radio stars. At 178 MHz, Cygnus A, one of the brightest radio sources, has been measured to have an intensity of $I = 8.1\ kJy$ [29] (link to database). The LOFAR SEFD at 178 MHz is published to be ~3.5 kJy on their website. This would allow phase information from Cygnus A to be measured to a precision of $\sigma_\phi \approx 0.2\ m$. For the same sized debris and environmental conditions as above but at 178 MHz, $|\delta\phi| \approx 0.002\ m$. Even though the effect on the phase is much larger at lower frequencies, the noise at HF bands is significantly higher.

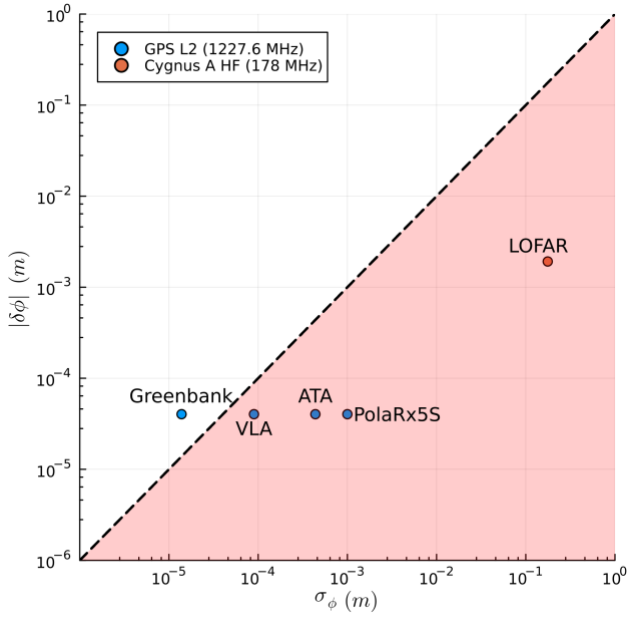

Fig. 2: Predicted phase advance generated by the wake from a 5 cm sized debris moving through daytime F-layer during solar maximum as observed by different combinations of sensors and frequencies. The dashed line is where $\delta\phi = \sigma_\phi$. The red hued section is where $\sigma_\phi > \delta\phi$ making refractive effects unobservable.

Fig. 2 summarizes the above discussion. The Greenbank and VLA are expected to marginally be able to observe the wakes from a 5 cm sized object under best case conditions. The location of the sensors in this diagram is specific to the debris size. For larger debris sizes, $|\delta\phi|$ increases.

3. SCATTERING EFFECTS

The carrier signal will also scatter off the local plasma structure. The secondary scattered GNSS signal may be detectable even when the refractive effect is negligible.

For a classical hard radar target, the scattering cross section is governed by the ratio of the size of the object to the wavelength a/λ, where a is a characteristic size of the object and λ is the wavelength being used. Objects much smaller than the wavelength, such as space debris to any radio wavelength, are Rayleigh scattered with a cross section given by Eqn. 3.1. A is the projected area of the object.

$$\sigma_{Rayleigh} = \frac{4\pi A^2}{\lambda^2} \tag{3.1}$$

The ionospheric plasma structures which form around a spacecraft are not a hard radar target. As originally presented in [30,31] the scattering of radio waves off an plasma wake from a conducting sphere can be described in CGS-Gaussian units by Eqn. 3.2. This formulation neglects magnetic fields. $\boldsymbol{q} = \boldsymbol{k}' - \boldsymbol{k}$ which are respectively the outgoing ($\boldsymbol{k}'$) and incoming wavevectors ($\boldsymbol{k}$).

$$\sigma(\psi,\theta) = \left\{\frac{1}{16}\left(\frac{\omega_p}{c}\right)^4 \frac{R_0^4 \sin^2\psi_1}{q^2}\right\} F(a_0,\theta)|G(qR_0,\cos\theta)|^2 \tag{3.2}$$

$F(a_0,\theta)$ describes the length of the plasma wake due to the ion acoustic Mach number (a_0) and the angle between the velocity of the object and $\boldsymbol{q}$ (θ). $|G|$ is a geometrical factor which accounts for the debris not being a point mass. We assume the debris is a sphere. At the Mach number increases, the wake structure becomes longer. That in turn increases the anisotropy of the scattering cross section. The magnitude of $\boldsymbol{q}$ is $q = 2k\sin(\psi/2)$, where ψ is the angle between the incident and scattered wavevector. ψ_1 is the angle between the incident electric field and reflected

wavevector. For a circularly polarized signal, we neglect this term. GPS carrier signals are right hand circularly polarized.

$$F(a_0,\theta)=\frac{\frac{\pi}{4}a_0^2\exp(-2a_0^2\,cos^2\,\theta)+[a_0W(a_0\cos\theta)]^2}{\frac{\pi}{4}a_0^2\cos\theta\exp(-2a_0^2\,cos^2\,\theta)+[1-a_0\cos\theta\,W(a_0\cos\theta)]^2} \tag{3.3}$$

$W(x)\triangleq e^{-x^2}\int_0^x e^{t^2}dt=\frac{\sqrt{\pi}}{2}\mathrm{erfi}(x)\exp(-x^2)$. When computing this function, it was attempted to compute $W(x)$ using both a trapezoidal rule integral and a preexisting library for computing error functions. The trapezoidal rule version of the integral was significantly less accurate that using a preexisting imaginary error function such as in the SpecialFunctions.jl library.

$$G(x,\theta)=2\int_0^{\frac{\pi}{2}}\cos\nu\sin\nu\exp[ix\cos\nu\cos\theta]\,J_0(x\sin\nu\sin\theta)\,d\nu \tag{3.4}$$

The G function in Eqn. 2.1 is given above. J_0 is a zero order Bessel function of the first kind. This term adds in the geometric effect of a finite sized sphere. These results can be derived by considering first the scattered wave from a region with a different index of refraction. The scattered wave is the integral over the dipole radiation that is emitted from the plasma region. The dipole moment in the plasma is induced by the incident wake. As before in this paper, $\boldsymbol{q}\equiv\boldsymbol{k}'-\boldsymbol{k}$ and primed quantities indicate scattered fields. $\bar{\varepsilon}$ is the dielectric constant at the receiver. On the surface of the Earth $\bar{\varepsilon}=1$ in Gaussian units.

$$\boldsymbol{E}'=\frac{e^2}{m\omega^2\bar{\varepsilon}}\frac{e^{i\boldsymbol{k}\cdot\boldsymbol{r}}}{r}\left(\boldsymbol{k}'\times(\boldsymbol{k}'\times\boldsymbol{E_0})\right)n_q \tag{3.5}$$

$$n_q\equiv\int\delta n(\boldsymbol{r})\exp(-i\boldsymbol{q}\cdot\boldsymbol{r})\,d^3r \tag{3.6}$$

Definitionally, $d\sigma=\frac{1}{16\,\pi^2\varepsilon^2}\left(\frac{\omega_p}{\omega}\right)^4\left(\frac{|n_q|}{n_0}\right)^2k^4\sin^2\psi_1\,d\Omega$, where $d\Omega$ is a differential of solid angle. $\varepsilon=1-\frac{4\pi ne^2}{m\omega^2}$. As shown in [17], it is easiest to calculate n_q directly from the Fourier transform of the velocity distribution function perturbation, i.e. $n_q=\int\delta f_q\,d^3v$. More details on deriving Eqn. 3.2, including an expression for n_q from a solution to the plasma wake can be found in [17].

The ratio of the receiver power from the scatterer and the transmitter is of interest for characterizing the feasibility of observing the scattered GNSS signal. Eqn. 3.7 shows the expected power at the receiver. R_1 is the distance from the transmitter to the scattered and R_2 is the distance from the scatterer to the receiver. G_r and G_t are respectively the receiver and transmitter gain.

$$P_{r,scat}=\frac{G_tG_r\lambda^2\sigma_s}{(4\pi)^3R_1^2R_2^2}P_t \tag{3.7}$$

Similarly, we can define a received power for the direct signal in Eqn. 3.8. R is the direct distance from the transmitter to the receiver.

$$P_{r,direct}=\frac{G_tG_r\lambda^2}{(4\pi)^2R^2}P_t \tag{3.8}$$

Dividing Eqn. 3.7 by 3.8 while assuming $R=R_1+R_2$ and $\frac{R_2}{R_1}\ll1$ yields Eqn. 3.9. Assuming $R=R_1+R_2$ is most valid when the scattering angle is small. For the 25.19 MHz scatter, this is not true.

$$\frac{P_{r,scat}}{P_{r,direct}}=\frac{\sigma_s}{4\pi R_2^2}=\frac{\sigma_s}{4\pi R_{scat}^2} \tag{3.9}$$

At the receiver, the scattered signal will manifest as a multipath effect. The relative strength of the second signal will be $\frac{P_{r,scat}}{P_{r,direct}}=\frac{\sigma_s}{4\pi R_{scat}^2}$ if it is assumed that the distance from the receiver to the transmitter is much larger than the

receiver to the scatterer. R_{scat} is the distance from the scattering to the receiver. An additional gain is added to compensate for the signal being stronger at the scatterer than equivalently at the surface. This gain = $1/(1 - R_{scat}/R_{direct})^2$. It is equal to 0.18 dB for a scatterer at 400 km.

Fig. 3 shows the forward scattering cross section of a 5 cm radius sphere with a plasma wake for small scattering angles while varying the angle with respect to the wake direction. It is assumed that the incident wave comes from zenith and that the plasma frequency ω_p is a constant 10 MHz. The scatterer is assumed to be in a circular orbit with a speed given by $v = \sqrt{\frac{\mu_g}{R_{scat}+R_{Earth}}}$ where μ_g is the gravitational parameter of the Earth. At sea level (altitude=0 m), this angle corresponds to a 7.3 m projected distance on the ground. The Rayleigh cross section of the same sized object is $\sigma_R = 0.009\ m^2$. In this case, the plasma wake and the debris itself have comparable cross sections.

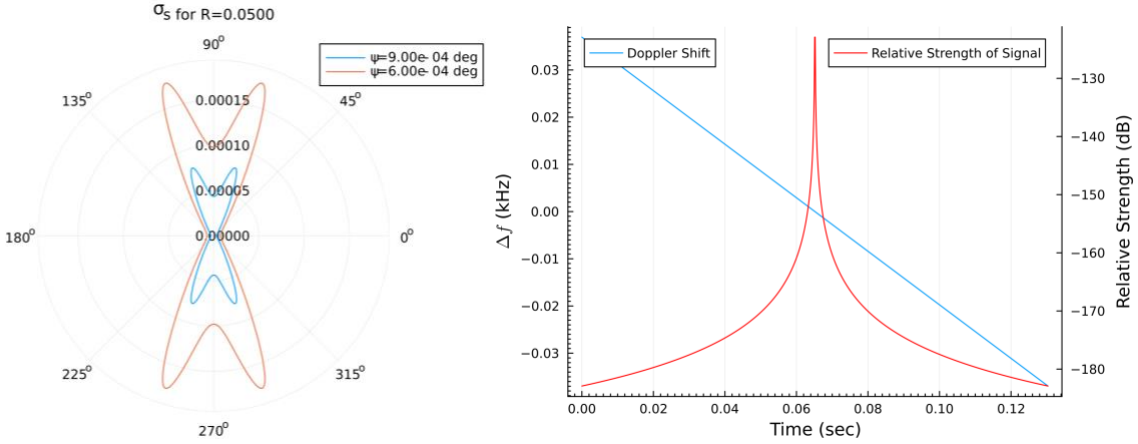

Fig. 3: Scattering cross section for small scattering angle of 5 cm sized sphere at GPS L1 frequency. 0°points along the velocity vector of the debris. The debris is assumed to be at 400km altitude.

It has been proposed that such receivers can accomplish 166 dB gain under special processing conditions [32]. This indicates that the scattered signal from a 5 cm object would be detectable at this small scattering angle. Since the scattering cross section is continuous in ψ (the scattering angle), we can find a scattering angle which accomplishes a -150 dB gain. We then equate that to a radius of the lobe on the ground as $r = R_{scat} \tan \psi_{-150\,dB}$. Fig. 4 shows that, for these high processing gain systems, the scattered signal should be detectable in the upper centimeter range. At -200 dB, millimeter sized objects would detectable over a region 3 cm in radius on the ground. The relationship between radius of lobe size and debris radius is a power law. For a 1 m radius lobe at -200 dB, a 7 mm radius debris would be the smallest object to scatter over that area.

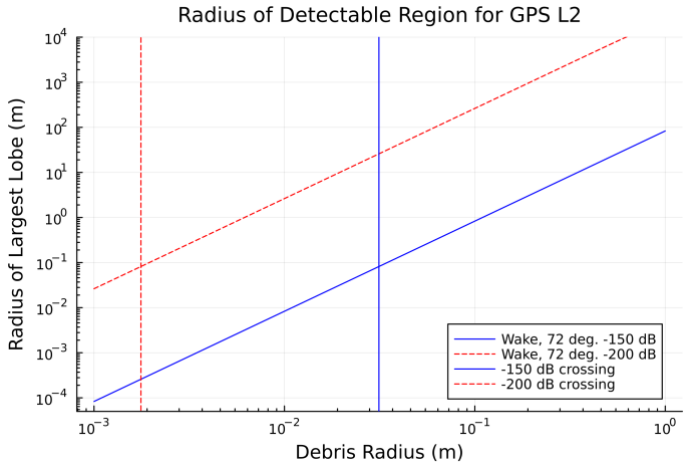

Fig. 4: Size of scattered region on Earth for various signal strengths. The altitude of the debris is assumed to be 400 km. The vertical lines indicate for a given relative signal size where the ionized tail cross section is the same size as the Rayleigh cross section. For debris with a radius to the left of the vertical line, the ionized tail would be the larger cross section.

For the same relative signal strengths, Fig. 5 shows the same calculation on 25.19 MHz. Sub-centimeter debris would be detectable at the -200 dB level over areas 10's of meters across. It should be noted that the LOFAR radio telescope, which observed ionospheric scintillation patterns [16], has a main array with antennas spaced about that distance apart.

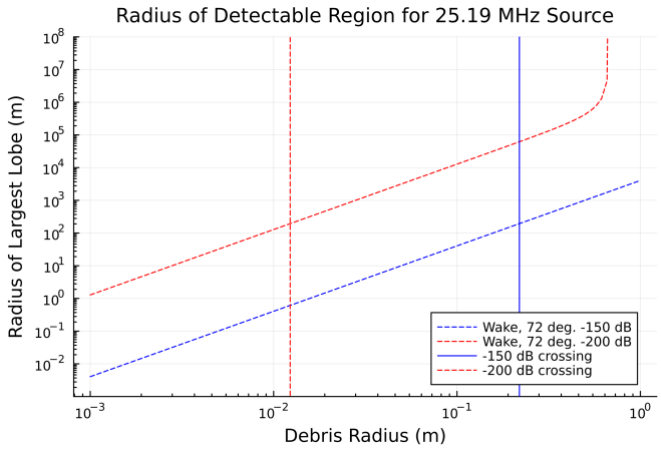

Fig. 5: Size of scattered region on Earth for various signal strengths receiving at 25.19 MHz. The altitude of the debris is assumed to be 400 km. Vertical lines indicate the debris size where the Rayleigh scattering relative signal strength is the same as the plasma wake cross section.

The nonlinear behavior of the -200 dB wake scattering at high debris radius in Fig. 5 is due to the magnitude of the scattered signal being above -200 dB for all angles.

Solitons:

Eqn. 3.10 describes for forward-scattered cross-section of a Gaussian electron density perturbation of characteristic size ρ_0 in CGS Gaussian units as derived by [30]. The frequency dependence only manifests for $\psi \neq 0$.

$$\sigma_s(0) \approx \frac{4\pi^4 e^4 \rho_0^6}{m_e^2 c^4} \Delta N^2 \tag{3.10}$$

In the ion acoustic formulation of a plasma soliton (as opposed to one including magnetic effects, see [8]), the maximum density perturbation and characteristic size are related by: $\left(\frac{\rho_0}{\lambda_D}\right)^2 \frac{\Delta N}{N_0} = C$, where C is a constant. Plugging this relationship into Eqn. 3.11 yields an estimate of the forward cross-section for an ion acoustic soliton of magnitude ΔN where ΔN is in units of N_0. Solitons are distinctly not Gaussian shaped, so this is a further approximation.

$$\sigma_s(0) \approx \frac{4\pi^4 e^4 \lambda_D^6}{m_e^2 c^4} \mathrm{C}^3 \Delta N^{-2} \approx 3.1 \times 10^{-23} C^3 \lambda_D^6 N_0^3 \Delta N^{-2} \tag{3.11}$$

Taking $C = 1$, which is the same order of magnitude with what is reported in [33] and assuming that the density perturbation scales with the background density, i.e. $\Delta N = N_0 U$, where U is dimensionless, the cross section scales in altitude as $\sigma = \mathcal{O}(\lambda_D^6 N_0)$. As can be seen in Fig. 6, the highest scattering cross section occurs at the highest altitude. This is driven by the Debye length increasing with altitude. If $U \approx 1$, then at 2000 km $\sigma_s(0) \approx 0.03\ m^2$ making $P_{scat}/P_{direct} = -152$ dB. $2000\ km$ is the upper bound for the IRI environmental model.

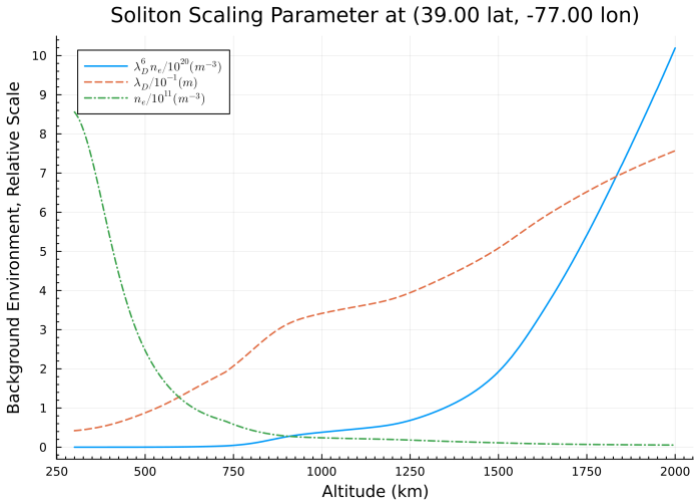

Fig. 6: Soliton scaling parameter ($\lambda_D^6 N_0$) calculated using the 2020 IRI evaluated on 24-09-1998, 19:00:00 UT over approximately College Park, MD.

The upper ionosphere (>1500 km) and middle Earth orbit (MEO, $2{,}000 \leq h \leq 9{,}000$ km) are the expected regions of ion acoustic precursor soliton generation [1]. Serendipitously, the forward scattering cross section also increases to the threshold of detectability at these altitudes. Preliminarily, this would indicate that precursor solitons at high altitudes may also be detectable in a similar manner to plasma wakes. Since the forward scattering relation does not include frequency dependence and assumes a different analytical form than a soliton, this result needs to be refined.

4. NETWORK GEOMETRY

As seen in Fig. 4 and Fig. 5, the point of intersection along the debris radius axis between the crossover point where the plasma wake has a larger cross section than the Rayleigh cross section has the same lobe size regardless of the maximum signal loss considered. We shall use this result to inform the network geometry.

Table 2: Characteristic scattering lobe sizes for various signal types when the wake cross section is the same size as the Rayleigh scattered cross section of the debris.

Signal Used	Characteristic Wake Scattering Lobe Size
GPS L2	40 cm
Cassiopeia 25 MHz emission	700 meters

Table 3 shows a non-exhaustive list of current GPS TEC stations with multiple receivers. The receivers at these stations are placed too far apart to resolve the lobes from GPS L2 scattering.

Table 3: Existing observatories with GNSS receivers. Inter-receiver distances are estimated using the Google Maps range tool and diagrams of the site.

Station	Receiver Spacing	Source
Goddard Geophysical and Astronomical Observatory	~50 meters	https://space-geodesy.nasa.gov/NSGN/sites/GGAO/GGAO.html
McDonald Geophysical Observatory (3 GNSS stations)	~70 meters	https://www.haystack.mit.edu/geodesy/geodesy-projects/co-located-techniques-and-atmospheric-ties/
Allen Telescope Array	~10-25 meters	https://www.seti.org/ata-technical-overview

To study the scattering pattern from debris, multiple receivers that could resolve the lobes of the scattering pattern would be needed. At two current observatories (listed in Table 3), it would be possible to observe the debris passing over the station without resolving the scattering pattern if it was in a suitable orientation. In a hypothetical system

which used a HF emission as the source, the current arrangement of GNSS monitoring stations at these two observatories would be sufficient to resolve the lobes of the scattering pattern.

An improved monitoring network could be co-located at the observatories in Table 3 or other ionospheric monitoring sites. Such a network would include a grid of receivers with an inter-receiver spacing below the characteristic lobe size.

5. A PROPOSED EXPERIMENT

In any of the scenarios considered, disentangling noise from a successful detection will be the main challenge. A buildup of a network of monitoring stations to track small debris should be done in stages to examine the physics. As a first step, we propose simultaneously looking for a large target through multiple methods. For example, the International Space Station will have a significant scatter area for GPS carrier signals. The Rayleigh cross section of the ISS is larger than its plasma wake cross section $\left(\sigma_R \approx \frac{4\pi(100\ m \times 70\ m)^2}{(20cm)^2} = 1.5 \times 10^{10}\ m^2, \sigma_{wake} \approx 10^8\ m^2 \text{ for the angles in Fig. } 4\right)$. The relative strength of scattered GPS L1 would be -21.4 dB and scattering pattern on the ground will not exhibit the butterfly pattern seen above with the wake scattering. This would be sufficient to establish the technique of detecting weak GPS scatter.

However, a nonnegligible refractive effect will also be exhibited. Fig. 7 shows a probabilistic estimate of the phase delay on GPS L2. Even during solar minimum, this should be within the measurement range of ionospheric monitoring GNSS receivers.

Since the data is sparse, a probabilistic view is taken. The width is taken to lie in a Gaussian probability density function (pdf) with a standard deviation 200 meters centered around 300 meters. The background electron density statistics are taken from the IRI 2020 model forecasting the electron density at midnight at 10 degrees latitude, 110 degrees longitude, and altitude 410 km on January 1st of every year from 1961 to 2021. These densities are fit to a 6th order Gaussian mixture model and presented in the bottom subplot of Fig. 7. This captures the wide variation in electron density which occurs in the ionosphere due to the solar 11-year solar cycle. The joint pdf is calculated as $p_{joint}(w, n_{e,background}) = p_{width}(w) * p_{n_e}(n_{e,background})$. The yellow contours in Fig. 7 show the regions of maximum joint probability. The phase advance from the variation in TEC is calculated as $\delta\rho = \kappa\frac{\delta TEC}{f^2}$. The phase advance for GPS L2 frequency is shown in Fig. 7. The phase advance from the ISS wake will be between 5 and 50 mm, depending most strongly on the portion of the solar cycle the observation is taken in. Either carrier phase change should be detectable by an ionospheric reference receiver.

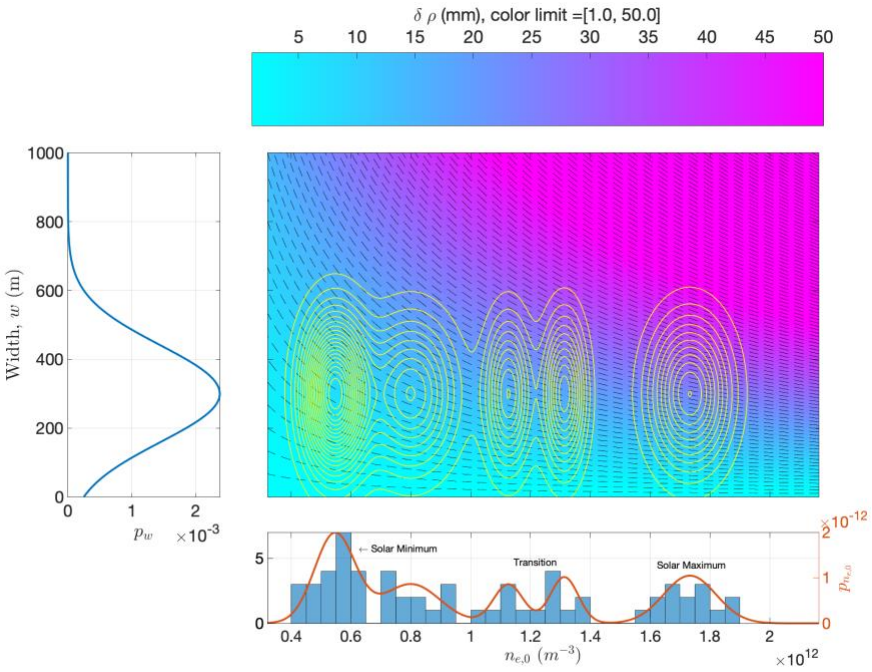

Fig. 7: Prediction of refractive phase delay in GPS L2 carrier frequency. The L1 carrier frequency will also have a phase delay proportional and of similar magnitude to the L2 carrier frequency phase delay.

Table 4 lists some publicly accessible GNSS monitoring networks. It would be advantageous to execute an experiment correlating an ISS pass through the GNSS satellite-to-station line with a carrier frequency-dependent phase delay observed by one of the stations in this network. Such an experiment would demonstrate that GNSS carrier signals are modified by local plasma structures in the ionosphere that originate with spacecraft interactions.

Table 4: GNSS monitoring station networks with publicly available data.

Network	Geographic Coverage	Number of Stations	Maximum Data Rate (Hz)
INGV eSWua [34]	Mediterranean Sea, Antarctica, Europe[1]	21	0.1
CHAIN [35]	Canadian High Arctic	26	50
NOAA/NDS CORS [36]	Continental US, Alaska, Hawaii, Iraq	2729	0.03[2]
IGS/NASA CDDIS	Worldwide	312[3]	1
GNET [37]	Greenland	30	20[4]

6. CONCLUSIONS

Considering a space-based radio source, we have shown that the signal scattered by the plasma wake of a sub-centimeter space debris is larger than the signal scattered by the debris directly. Bi-static GNSS radar approaches to detecting sub-cm debris may be more effective than previously thought because of this phenomenon. For frequencies lower than L-band GNSS signals, the scattering effect is more pronounced. A 25.19 MHz signal, which was observed originating from the Cassiopeia A system, would scatter over a region of kilometers in size. A benefit of this detection approach is that it is not necessary to build new transmitters, as both GNSS and natural radio sources are plentiful. Additionally, existing GNSS reference station sites could be reused for this application.

[1] Has sparse worldwide coverage as well.
[2] At device sample rate is available on request. However, after 30 days the publicly available data is decimated to a 30 second sample rate.
[3] For 1 second data in 2023.
[4] High-rate data is removed after about a month depending on the exact format, although this seems inconsistently done when viewing their database.

Further, some sites may already produce some data that could be used to test this technique. There is also a refractive effect which scales with the size of the object. We predict that existing radio telescopes are sensitive to this effect at GNSS frequencies for sub centimeter debris. For larger objects, existing GNSS ionospheric reference receivers may be sufficient to observe the effect. Since both scattering and refraction are premised on the assumption that the plasma wake of the debris/spacecraft affects radio transmission, we also proposed an experiment that uses the refractive case to test the feasibility of observing the ISS wake using ground based GNSS receivers.

7. REFERENCES

[1] Truitt, A. S., and Hartzell, C. M. "Simulating Plasma Solitons from Orbital Debris Using the Forced Korteweg–de Vries Equation." *Journal of Spacecraft and Rockets*, Vol. 57, No. 5, 2020, pp. 876–897. https://doi.org/10.2514/1.A34652.

[2] Sen, A., Tiwari, S., Mishra, S., and Kaw, P. "Nonlinear Wave Excitations by Orbiting Charged Space Debris Objects." *Advances in Space Research*, Vol. 56, No. 3, 2015, pp. 429–435. https://doi.org/10.1016/j.asr.2015.03.021.

[3] Wilson, C. M., and Hartzell, C. M. Simulated Propagation of Ion Acoustic Solitary Waves from Orbital Debris Contrasted with Simultaneous Observations of the Ionosphere by an Incoherent Scatter Radar. 2023.

[4] Bernhardt, P., Scott, L., and Howarth, A. Space Object Identification by In Situ Measurements of Orbit-Driven Waves (SOIMOW). 64th Annual Meeting of the APS Division of Plasma Physics, Spokane, WA, Oct 17, 2022.

[5] Davies, K. *Ionospheric Radio*. Institution of Engineering and Technology, 1990.

[6] Truitt, A. S., and Hartzell, C. M. "Simulating Damped Ion Acoustic Solitary Waves from Orbital Debris." *Journal of Spacecraft and Rockets*, Vol. 57, No. 5, 2020, pp. 975–984. https://doi.org/10.2514/1.A34674.

[7] Truitt, A. S., and Hartzell, C. M. "Three-Dimensional Kadomtsev–Petviashvili Damped Forced Ion Acoustic Solitary Waves from Orbital Debris." *Journal of Spacecraft and Rockets*, Vol. 58, No. 3, 2021, pp. 848–855. https://doi.org/10.2514/1.A34805.

[8] Sen, A., Mukherjee, R., Yadav, S. K., Crabtree, C., and Ganguli, G. "Electromagnetic Pinned Solitons for Space Debris Detection." *Physics of Plasmas*, Vol. 30, No. 1, 2023, p. 012301. https://doi.org/10.1063/5.0099201.

[9] Henderson, C. L., and Samir, U. "Observations of the Disturbed Region around an Ionospheric Spacecraft." *Planetary and Space Science*, Vol. 15, No. 10, 1967, pp. 1499–1513. https://doi.org/10.1016/0032-0633(67)90083-9.

[10] André, M., Eriksson, A. I., Khotyaintsev, Y. V., and Toledo-Redondo, S. "The Spacecraft Wake: Interference With Electric Field Observations and a Possibility to Detect Cold Ions." *Journal of Geophysical Research: Space Physics*, Vol. 126, No. 9, 2021, p. e2021JA029493. https://doi.org/10.1029/2021JA029493.

[11] Ekers, R. D., van Gorkom, J. H., Schwarz, U. J., and Goss, W. M. "The Radio Structure of SGR A." *Astronomy and Astrophysics*, Vol. 122, 1983, pp. 143–150.

[12] Kraus, J. D., Ko, H. C., and Matt, S. "Galactic and Localized Source Observations at 250 Megacycles per Second." *The Astronomical Journal*, Vol. 59, 1954, pp. 439–443. https://doi.org/10.1086/107059.

[13] Arias, M., Vink, J., De Gasperin, F., Salas, P., Oonk, J. B. R., Van Weeren, R. J., Van Amesfoort, A. S., Anderson, J., Beck, R., Bell, M. E., Bentum, M. J., Best, P., Blaauw, R., Breitling, F., Broderick, J. W., Brouw, W. N., Brüggen, M., Butcher, H. R., Ciardi, B., De Geus, E., Deller, A., Van Dijk, P. C. G., Duscha, S., Eislöffel, J., Garrett, M. A., Grießmeier, J. M., Gunst, A. W., Van Haarlem, M. P., Heald, G., Hessels, J., Hörandel, J., Holties, H. A., Van Der Horst, A. J., Iacobelli, M., Juette, E., Krankowski, A., Van Leeuwen, J., Mann, G., McKay-Bukowski, D., McKean, J. P., Mulder, H., Nelles, A., Orru, E., Paas, H., Pandey-Pommier, M., Pandey, V. N., Pekal, R., Pizzo, R., Polatidis, A. G., Reich, W., Röttgering, H. J. A., Rothkaehl, H., Schwarz, D. J., Smirnov, O., Soida, M., Steinmetz, M., Tagger, M., Thoudam, S., Toribio, M. C., Vocks, C., Van Der Wiel, M. H. D., Wijers, R. A. M. J., Wucknitz, O., Zarka, P., and Zucca, P. "Low-Frequency Radio Absorption in Cassiopeia A." *Astronomy & Astrophysics*, Vol. 612, 2018, p. A110. https://doi.org/10.1051/0004-6361/201732411.

[14] Bietenholz, M. F., Kassim, N., Frail, D. A., Perley, R. A., Erickson, W. C., and Hajian, A. R. "The Radio Spectral Index of the Crab Nebula." *The Astrophysical Journal*, Vol. 490, No. 1, 1997, p. 291. https://doi.org/10.1086/304853.

[15] Abdo, A. A., Ackermann, M., Ajello, M., Atwood, W. B., Baldini, L., Ballet, J., Barbiellini, G., Bastieri, D., Baughman, B. M., Bechtol, K., Bellazzini, R., Berenji, B., Blandford, R. D., Bloom, E. D., Bonamente, E., Borgland, A. W., Bouvier, A., Brandt, T. J., Bregeon, J., Brez, A., Brigida, M., Bruel, P., Buehler, R., Buson,

S., Caliandro, G. A., Cameron, R. A., Cannon, A., Caraveo, P. A., Carrigan, S., Casandjian, J. M., Cavazzuti, E., Cecchi, C., Çelik, Ö., Charles, E., Chekhtman, A., Cheung, C. C., Chiang, J., Ciprini, S., Claus, R., Cohen-Tanugi, J., Colafrancesco, S., Cominsky, L. R., Conrad, J., Costamante, L., Davis, D. S., Dermer, C. D., Angelis, A. de, Palma, F. de, Silva, E. do C. e, Drell, P. S., Dubois, R., Dumora, D., Falcone, A., Farnier, C., Favuzzi, C., Fegan, S. J., Finke, J., Focke, W. B., Fortin, P., Frailis, M., Fukazawa, Y., Funk, S., Fusco, P., Gargano, F., Gasparrini, D., Gehrels, N., Georganopoulos, M., Germani, S., Giebels, B., Giglietto, N., Giommi, P., Giordano, F., Giroletti, M., Glanzman, T., Godfrey, G., Grandi, P., Grenier, I. A., Grondin, M.-H., Grove, J. E., Guillemot, L., Guiriec, S., Hadasch, D., Harding, A. K., Hase, H., Hayashida, M., Hays, E., Horan, D., Hughes, R. E., Itoh, R., Jackson, M. S., Jóhannesson, G., Johnson, A. S., Johnson, T. J., Johnson, W. N., Kadler, M., Kamae, T., Katagiri, H., Kataoka, J., Kawai, N., Kishishita, T., Knödlseder, J., Kuss, M., Lande, J., Latronico, L., Lee, S.-H., Lemoine-Goumard, M., Garde, M. L., Longo, F., Loparco, F., Lott, B., Lovellette, M. N., Lubrano, P., Makeev, A., Mazziotta, M. N., McConville, W., McEnery, J. E., Michelson, P. F., Mitthumsiri, W., Mizuno, T., Moiseev, A. A., Monte, C., Monzani, M. E., Morselli, A., Moskalenko, I. V., Murgia, S., Müller, C., Nakamori, T., Naumann-Godo, M., Nolan, P. L., Norris, J. P., Nuss, E., Ohno, M., Ohsugi, T., Ojha, R., Okumura, A., Omodei, N., Orlando, E., Ormes, J. F., Ozaki, M., Pagani, C., Paneque, D., Panetta, J. H., Parent, D., Pelassa, V., Pepe, M., Pesce-Rollins, M., Piron, F., Plötz, C., Porter, T. A., Rainò, S., Rando, R., Razzano, M., Razzaque, S., Reimer, A., Reimer, O., Reposeur, T., Ripken, J., Ritz, S., Rodriguez, A. Y., Roth, M., Ryde, F., Sadrozinski, H. F.-W., Sanchez, D., Sander, A., Scargle, J. D., Sgrò, C., Siskind, E. J., Smith, P. D., Spandre, G., Spinelli, P., Starck, J.-L., Stawarz, L., Strickman, M. S., Suson, D. J., Tajima, H., Takahashi, H., Takahashi, T., Tanaka, T., Thayer, J. B., Thayer, J. G., Thompson, D. J., Tibaldo, L., Torres, D. F., Tosti, G., Tramacere, A., Uchiyama, Y., Usher, T. L., Vandenbroucke, J., Vasileiou, V., Vilchez, N., Vitale, V., Waite, A. P., Wang, P., Winer, B. L., Wood, K. S., Yang, Z., Ylinen, T., and Ziegler, M. "FERMI LARGE AREA TELESCOPE VIEW OF THE CORE OF THE RADIO GALAXY CENTAURUS A." *The Astrophysical Journal*, Vol. 719, No. 2, 2010, p. 1433. https://doi.org/10.1088/0004-637X/719/2/1433.

[16] Fallows, R. A., Forte, B., Astin, I., Allbrook, T., Arnold, A., Wood, A., Dorrian, G., Mevius, M., Rothkaehl, H., Matyjasiak, B., Krankowski, A., Anderson, J. M., Asgekar, A., Avruch, I. M., Bentum, M., Bisi, M. M., Butcher, H. R., Ciardi, B., Dabrowski, B., Damstra, S., Gasperin, F. de, Duscha, S., Eislöffel, J., Franzen, T. M. O., Garrett, M. A., Grießmeier, J.-M., Gunst, A. W., Hoeft, M., Hörandel, J. R., Iacobelli, M., Intema, H. T., Koopmans, L. V. E., Maat, P., Mann, G., Nelles, A., Paas, H., Pandey, V. N., Reich, W., Rowlinson, A., Ruiter, M., Schwarz, D. J., Serylak, M., Shulevski, A., Smirnov, O. M., Soida, M., Steinmetz, M., Thoudam, S., Toribio, M. C., Ardenne, A. van, Bemmel, I. M. van, Wiel, M. H. D. van der, Haarlem, M. P. van, Vermeulen, R. C., Vocks, C., Wijers, R. A. M. J., Wucknitz, O., Zarka, P., and Zucca, P. "A LOFAR Observation of Ionospheric Scintillation from Two Simultaneous Travelling Ionospheric Disturbances." *Journal of Space Weather and Space Climate*, Vol. 10, 2020, p. 10. https://doi.org/10.1051/swsc/2020010.

[17] Al'pert, Y. *Space Physics with Artificial Satellites / Iskusstvennye Sputniki V Razrezhennoi Plazme / СПУТНИКИ В РАЗРЕЖЕННОИ ПЛАЗМЕ*. Springer New York, NY.

[18] Kraus, J. D., and Dreese, E. E. "Sputnik I's Last Days in Orbit." *Proceedings of the IRE*, Vol. 46, No. 9, 1958, pp. 1580–1587. https://doi.org/10.1109/JRPROC.1958.286933.

[19] Kraus, J. D., Higgy, R. C., Scheer, D. J., and Crone, W. R. "Observations of Ionization Induced by Artificial Earth Satellites." *Nature*, Vol. 185, No. 4712, 1960, pp. 520–521. https://doi.org/10.1038/185520a0.

[20] Kraus, J. D., Higgy, R. C., and Albus, J. S. "Observations of the U.S. Satellites Explorers I and III by CW Reflection." *Proceedings of the IRE*, Vol. 46, No. 8, 1958, pp. 1534–1542. https://doi.org/10.1109/JRPROC.1958.286975.

[21] Gerson, N. C. "Radio Wave Propagation from Sputnik III." *Journal of Atmospheric and Terrestrial Physics*, Vol. 25, No. 12, 1963, pp. 699–706. https://doi.org/10.1016/0021-9169(63)90063-1.

[22] Hame, T. G., and Stuart, W. D. The Detection of Artificial Satellites by Their Influences on the Ionosphere. In *Interactions of Space Vehicles with an Ionized Atmosphere* (S. F. Singer, ed.), Pergamon, 1965, pp. 373–388.

[23] Mahmud, M., Qaisar, S., and Benson, C. Tracking Low Earth Orbit Small Debris with GPS Satellites as Bistatic Radar. Presented at the Advanced Maui Optical and Space Surveillance Technologies Conference, Wailea, Maui, Hawaii, 2016.

[24] Petit, G., and Luzum, B. IERS Technical Note No. 36. Frankfurt am Main: Verlag des Bundesamts für Kartographie und Geodäsie, , 2010.

[25] Murphy, G. B., Reasoner, D. L., Tribble, A., D'Angelo, N., Pickett, J. S., and Kurth, W. S. "The Plasma Wake of the Shuttle Orbiter." *Journal of Geophysical Research: Space Physics*, Vol. 94, No. A6, 1989, pp. 6866–6872. https://doi.org/10.1029/JA094iA06p06866.

[26] Langley, R. GPS Receiver System Noise. GPSWorld, Jun, 1997.
[27] Imara, N. “EPFD Measurements on GPS and Iridium at the RPA.” *SETI ATA Memo #53*.
[28] Siemion, A. P. V., Bower, G. C., Foster, G., McMahon, P. L., Wagner, M. I., Werthimer, D., Backer, D., Cordes, J., and Van Leeuwen, J. “THE ALLEN TELESCOPE ARRAY FLY’S EYE SURVEY FOR FAST RADIO TRANSIENTS.” *The Astrophysical Journal*, Vol. 744, No. 2, 2012, p. 109. https://doi.org/10.1088/0004-637X/744/2/109.
[29] Bennett, A. S. “The Revised 3C Catalogue of Radio Sources.” *Memoirs of the Royal Astronomical Society*, Vol. 68, 1962, p. 163.
[30] Al’pert, Y. L. “Investigation of the Ionosphere and of the Interplanetary Gas with the Aid of Artificial Satellites and Space Rockets.” *Soviet Physics Uspekhi*, Vol. 3, No. 4, 1961, p. 479. https://doi.org/10.1070/PU1961v003n04ABEH003291.
[31] Al’pert, Y. L., Gurevich, A. V., and Pitaevskiĭ, L. P. “Effects Produced by an Artificial Satellite Rapidly Moving in the Ionosphere or in an Interplanetary Medium.” *Soviet Physics Uspekhi*, Vol. 6, No. 1, 1963, p. 13. https://doi.org/10.1070/PU1963v006n01ABEH003492.
[32] Benson, C. R. Enhancing Space Situational Awareness Using Passive Radar from Space Based Emitters of Opportunity. Presented at the 2014 Military Communications and Information Systems Conference (MilCIS), 2014.
[33] Jaiswal, S., Bandyopadhyay, P., and Sen, A. “Experimental Observation of Precursor Solitons in a Flowing Complex Plasma.” *Physical Review E*, Vol. 93, No. 4, 2016, p. 041201. https://doi.org/10.1103/PhysRevE.93.041201.
[34] Upper atmosphere physics and radiopropagation Working Group, Cesaroni, C., Marcocci, C., Pica, E., and Spogli, L. “Electronic Space Weather Upper Atmosphere Database (ESWua) - Total Electron Content (TEC) Data, Version 1.0: Collection of the Ionospheric Total Electron Content (TEC) Data and Products of the ESWua Database.” 2020. https://doi.org/10.13127/ESWUA/TEC.
[35] Jayachandran, P. T., Langley, R. B., MacDougall, J. W., Mushini, S. C., Pokhotelov, D., Hamza, A. M., Mann, I. R., Milling, D. K., Kale, Z. C., Chadwick, R., Kelly, T., Danskin, D. W., and Carrano, C. S. “Canadian High Arctic Ionospheric Network (CHAIN): CHAIN.” *Radio Science*, Vol. 44, No. 1, 2009, p. n/a-n/a. https://doi.org/10.1029/2008RS004046.
[36] US Department of Commerce, N. O. and A. A. NCN Homepage - National Geodetic Survey. https://geodesy.noaa.gov/CORS/index.shtml. Accessed Aug. 9, 2023.
[37] Winther, D. K. M. B., Malte Nordmann. Greenland GNSS Network. https://go-gnet.org/. Accessed Aug. 9, 2023.

8. AWKNOWLEDGEMENTS

This material is based upon work supported by the U.S. Department of Energy, Office of Science, Office of Advanced Scientific Computing Research, Department of Energy Computational Science Graduate Fellowship under Award Number DE-SC0021110.